Densification and preservation of ceramic nanocrystalline character by spark plasma sintering

R. Chaim*[1], R. Marder[1], C. Estournés[2] and Z. Shen[3]

Spark plasma sintering is a hot pressing technique where rapid heating by dc electric pulses is used simultaneously with applied pressure. Thus, spark plasma sintering is highly suitable for rapid densification of ceramic nanoparticles and preservation of the final nanostructure. A considerable portion of the shrinkage during densification of the green compact of nanoparticles in the first and intermediate stages of sintering occurs during heating by particle rearrangement by sliding and rotation. Further densification to the final stage of sintering takes place by either plastic yield or diffusional processes. Full densification in the final stage of sintering is associated with diffusional processes only. Nanoparticle sliding and rotation during heating may also lead to grain coalescence, with much faster kinetics than normal grain growth at higher temperatures. Based on existing models for particle rearrangement and sliding, the contributions of these processes in conjunction with nanoparticle properties and process parameters were highlighted.

Keywords: Spark plasma sintering, Densification, Nanoparticles, Particle sliding, Plastic yield, Grain growth, Ceramics, Oxides

Introduction

The relationship between microstructure and properties in polycrystalline materials is a well accepted concept in materials science and engineering. In this respect, nanocrystalline materials are expected theoretically to exhibit significant deviations in many material properties compared to those measured in their conventional counterparts; some of these deviations were experimentally confirmed.[1–5] However, incomplete densification at low sintering temperatures results in nanometric residual pores, where excessive sintering temperatures result in grain growth; both microstructure features affect the properties expected from theoretically dense nanocrystalline ceramics. Therefore, densification of the ceramic nanoparticles to fully dense nanocrystalline compacts has become a challenge in the last two decades. The novel techniques of spark plasma sintering (SPS) or field assisted sintering technology were successfully used for the rapid fabrication of many dense nanocrystalline oxides, and the reader is referred to the recent review papers on these topics.[6–8] However, due to the lack of full understanding of the electric field effect on the ceramic densification mechanisms and kinetics, most of the investigations still involve extensive densification experiments.

[1]Department of Materials Engineering, Technion – Israel Institute of Technology, Haifa 32000, Israel
[2]CNRS, Institut Carnot Cirimat, Toulouse Cedex 9 F-31602, France
[3]Department of Materials and Environmental Chemistry, Arrhenius Laboratory, Stockholm University, Stockholm S-10691, Sweden

*Corresponding author, email rchaim@technion.ac.il

In this paper, we used existing models for particle rearrangement and sliding, as well as grain coalescence and growth, to highlight their contribution during densification with respect to the ceramic nanoparticle characteristics and the SPS process parameters.

First and second stage sintering

It is well established that the main shrinkage during conventional sintering of nanoparticle compact starts at elevated temperatures, a few hundred degrees below the corresponding temperature of its conventional size counterpart powder. This effect is due to the high specific surface area and hence the high capillary forces acting on the nanoparticles. The main shrinkage in the second stage of sintering often occurs at temperatures high enough for the grain boundary (GB) and volume diffusion processes to take place. These expected capillary forces for the nanoparticles are in the order of several tens of megapascals, comparable to the external stresses generally applied during hot pressing/SPS of ceramic powders.[9] Nevertheless, significant densification is not achieved during pressureless heating at low heating rates; rapid surface diffusion during heating often leads to particle coarsening and partial sintering (neck formation) rather than to densification. The rapid heating with simultaneous pressure application during SPS lowers the onset temperature at which the maximum shrinkage rate occurs.[10,11] Consequently, most of the controlled SPS experiments in the literature reveal that the major densification of the ceramic nanoparticles occurs during the heating to the SPS temperature.[11–13] In the following sections, we will

DOI 10.1179/1743676111Y.0000000074

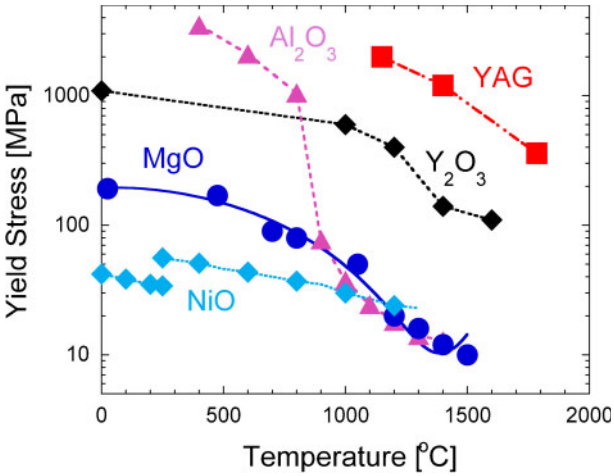

1 Yield stress of selected oxides versus temperature: at 100 MPa SPS pressure, NiO deforms at all temperatures where YAG is non-deformable even at 1800°C

discuss this observed rapid densification with respect to the nanoparticle and process characteristics.

Elastic hard nanoparticles

First, we will discuss the case of elastic hard ceramic nanoparticles, where no plastic deformation is expected, up to the isothermal SPS temperature.[13] This can be envisaged by following the change in yield stress of the ceramic material with the temperature (Fig. 1). Assuming that the yield stress of the oxide nanoparticles is similar to that of conventional single crystals, NiO may be deformed at all temperatures under the typical SPS pressure of 100 MPa, whereas no plastic deformation is expected in yttrium aluminium garnet [YAG ($Y_3Al_5O_{12}$)] up to 1800°C. The green density of the nanoparticles poured into the die (tap density or random loose packed) may vary within a wide range between 20 and 40%, depending on the degree of agglomeration. These values are much lower than the packing density expected for random close packing of uni-size spherical particles (64%). Much lower densities are expected with the deviation in nanoparticle aspect ratio from 1·0.[14] Therefore, even limited pressure applied at room temperature is expected to initiate densification by particle rearrangement by sliding and rotation. Similar to cold compaction of agglomerated powders, there is a threshold pressure that corresponds to the strength of the agglomerate, above which significant densification may be reached.[15,16] However, this pressure also depends on the nanoparticle morphology, size and distribution, as well as its chemical composition and hardness. Where spherical particles may rotate over each other, the faceted nanoparticles may impose significant frictional forces due to the large contact areas. The effect of the nanoparticle chemical composition is expressed by its coefficient of friction, which in turn is dictated by its surface chemical composition. Reduction in the particle size into the nanometre range is associated with the increase in the density of the solid/gas interfaces and the contact points per unit volume, hence the increase in the total work needed for the overall sliding of the nanoparticles. Consequently, sliding is expected only at a few regions at a time, where maximum free volume is available. Such nanoparticle systems are often characterised by jamming effect during densification.[17–19] In systems with attractive forces between the nanoparticles, the particle sliding may be arrested by jamming via crowding of fractal clusters.[17] A similar physical aspect of the powder consolidation was modelled by buckling of the arches of particles surrounding the closed pores in the green compact.[20]

Powder compaction may be treated by analysis of the Hertzian contacts between two spherical particles. The conditions in the random loose packed powder are close to that of oblique compression of two homogeneous and elastically isotropic spherical particles against each other. In the latter stages, when either the random loose packed state is jammed or the random close packed compact is formed, the problem is more of the normal Hertzian contact character. These pressing configurations were thoroughly treated and discussed by Walton.[21] He considered simultaneous application of normal and tangential stresses to the two particles. The normal stress component at the contact area between the particles is similar to that of the Hertzian contact, and the (normal) displacement of each particle centre along the line connecting the two particle centres is given by

$$w_0 = \frac{r_o^z}{R} \tag{1}$$

where r_o is the contact area radius, and R is the undeformed particle radius.

The effect of the shear stress component that is more complex should also be considered. When the spheres are first compressed and then sheared, the particle slip is confined to a circular annulus with radius $0<r<r_o$ at the contact area. Nevertheless, when the normal and shear stress components were simultaneously applied (oblique compression), if slip occurs, it leads to the sliding of the entire contact area. For a particle to slide, the ratio of shear u_0 to normal w_0 displacements of the sphere centre should obey[21]

$$\frac{u_0}{w_0} = f\frac{(1+C)}{2B} \tag{2}$$

where f is the friction coefficient, and B and C are parameters comprised of Lame's elastic constants $\mu=C_{44}$ and $\lambda=C_{12}$ of the particle material and are given by

$$B=\frac{1}{4\pi}\left(\frac{1}{\mu}+\frac{1}{\lambda+\mu}\right) \qquad C=\frac{1}{4\pi}\left(\frac{1}{\mu}-\frac{1}{\lambda+\mu}\right) \tag{3}$$

At first glance, equation (2) is independent of the particle size due to the homogeneous, elastic isotropy assumed for the particles. However, practically, as the particle size decreases into the nanometre range, the single crystal character of each nanoparticle is pronounced. Therefore, deviations are expected in equation (2) due to the particle size and consequent elastic anisotropy due to its orientation.

However, using equation (2), the problem may also be solved by superposition of the two stress components. In the event of lack of particle sliding, the increase in applied pressure is expected to result in either plastic yield or microcracking by radial compressive displacement normal to the contact area and the shear displacement perpendicular to the radial axis. Here, the assumption is that microcracking and/or fracture is initiated by a local yield, i.e. sessile dislocation interactions and void formation. The local yield is expressed by

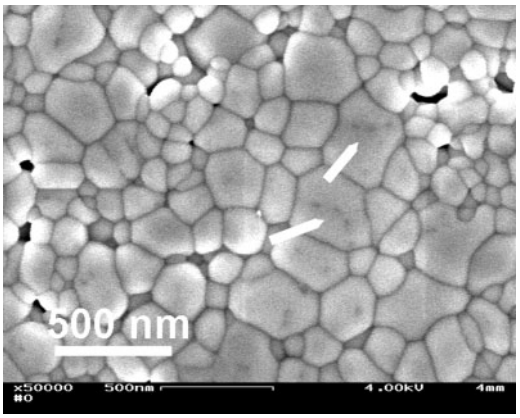

2 Scanning electron microscopy of thermally etched surface of nc-YAG reveals traces of LAGBs between nanoparticles that form larger grain clusters (arrowed): SPS performed for 5 min at 100 MPa and 1300°C

$$u_0 = \gamma_{\text{yield}} r \tag{4}$$

$$w_0 = \varepsilon_{\text{yield}} R \tag{5}$$

where γ_{yield} and $\varepsilon_{\text{yield}}$ are the shear and compressive yield strains at the contact area respectively.

Therefore, equations (2), (4) and (5) set the conditions for particle sliding. Regardless of the mechanism, these processes cause particles to slide since they change the particle morphology in the presence of the applied pressure in an irreversible manner. The onset condition and criteria for particle sliding is the yield or fracture. In this respect, the non-linear behaviour of the Hertzian contacts, under increasing pressures, during the indentation of ceramics, is related to the plastic deformation as well as to microcracking.

Yttrium aluminium garnet is a very high creep resistant oxide that can be used to demonstrate the sliding behaviour of the elastic and hard nanoparticles without yield. The deformation behaviour of YAG single crystals in various forms was characterised and exhibited brittle fracture at room temperature. A stress of 300 MPa was required for creep deformation of YAG single crystals at 1625°C ($0{\cdot}8T_{\text{m}}$).[22] The typical elastic modulus of 310 GPa and Vickers hardness of 15 GPa were reported.[23,24]

Several SPS experiments with YAG as hard ceramic nanoparticles examined the effect of pressure level and its application mode on the densification process.[25–27] An increase in the applied pressure at room temperature is expected to increase the green density in nanopowders, especially when the agglomerate strength is reached. However, the pore size and its distribution may be more important than the average green density. A systematic decrease in nanopore size and its volume fraction has been found with the increase in the cold isostatic pressing pressure (at 10–240 MPa) of the green YAG nanoparticle compacts, where the average green density was between 43 and 52%.[26] Two specimens cold isostatic pressed at 150 and 200 MPa, with 51 and 49% green densities, were sintered for 5 min at 1400°C and 90 MPa; they exhibited 94·5% density and 520 nm grain size versus 99·0% density and 340 nm grain size respectively. The comparative behaviour of the two specimens has shown extensive shrinkage in the former at low temperature (800°C) than at the SPS temperature. Since densification cannot account for the plastic yield at 800°C, it is mainly attributed to the particle sliding enhanced by surface diffusion.[25] This is in agreement with the faster densification rate observed at ~800°C for the same YAG nanoparticles with liquid forming LiF additive.[27] Consequently, effective sliding of hard nanoparticles at lower temperatures is expected to not only enhance densification but also provide conditions for enhanced grain coalescence and growth at the SPS temperature. The traces of low angle GBs (LAGBs) observed within the larger YAG grains (Fig. 2) resemble these consecutive processes.

On the other hand, the pressure application regime at high temperatures is yet important. Application of 100 MPa pressure, during heating, resulted at 1200°C with a narrow grain size distribution of ~615 nm.[28] In comparison, the application of the same pressure at the SPS isotherm (1400°C) resulted in a much wider and bimodal grain size distribution, with two mean grain sizes of ~250 and 1265 nm respectively. The latter microstructure development was related to the enhanced coarsening of the non-stressed nanoparticles via surface diffusion during heating up.

Using the volume based statistical mechanics approach, Kenkre *et al.* have formulated the density–pressure relation during compaction of powders.[29] The activation of the process (i.e. rearrangement or deformation) by pressure follows the exponential probability distribution, similar to thermal activation (Arrhenius type). Shrinkage, and hence density, depends exponentially on the applied pressure, as long as it takes place solely by particle rearrangement.[29] For a given applied pressure, there is an optimal SPS temperature at which maximal shrinkage rates are recorded in many systems during heating.[12,13,30] Likewise, an optimal applied pressure is also expected for full densification with minimal grain growth.

Plastic soft nanoparticles

The flow of nanoparticles can be described as similar to that of liquids. Therefore, the uniaxial pressure applied to the nanopowder confined in a die (as in SPS) can be described in terms of the effective hydrostatic pressure during SPS.[31] This pressure acts as a driving force for sliding/rotation of the particles at the sliding loci, whereas the capillary forces act as the driving force for particle sintering and coarsening at the non-sliding loci (i.e. jammed nanoparticles).

Powder compaction by plastic deformation at the particle contact points during cold and hot compaction was modelled for metallic systems[32–34] and may be applicable for plastically deformable ceramic nanoparticles.[31] Liu and DeLo[32] have shown that particle rearrangement by sliding may be active to a large extent for plastically deformable spherical particles up to compact densities of 92%. In this respect, the randomly closed packed powder, with 0·64 initial packing density, may experience more than ~15 and ~25% increase in packing density by particle rearrangement and plastic deformation respectively.

Schatt and co-workers[33,34] considered the formation of high dislocation density, at the deformed necks and particle surfaces, to serve as effective vacancy sinks. The particle and pore shape changes during densification were related to the reaction between the vacancies and

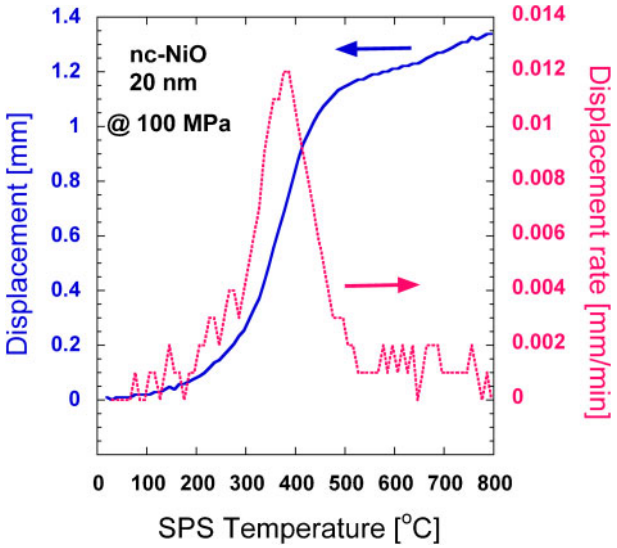

3 Ram displacement and its rate versus temperature at 100 MPa The sigmoidal shape curve (solid line) is characteristic of the shrinkage behaviour during densification by SPS. The highest shrinkage rate (dashed line) occurs during heating

dislocations in terms of viscous diffusion. Using Frenkel's model of shrinkage of a spherical pore by grain deformation, via vacancy diffusion from the pore, through the defective lattice, to the dislocation cores at the deformed necks (i.e. via dislocation climb), the relative volume shrinkage was expressed as[33]

$$\frac{\Delta V}{V} = -\frac{3\gamma_{sv}(1-\rho)}{r_p}\frac{D_l\Omega}{kTL^2}t \tag{6}$$

where V is the volume, γ_{sv} is the solid–vapour surface energy, ρ is the relative density, r_p is the average pore radius, D_l is the lattice diffusion coefficient of the slowest ion, Ω is the atomic volume of the slowest ion, k is Boltzmann's constant, T is the temperature, t is the time and L is the average distance between the dislocations.

The corresponding linear shrinkage rate for densification by sliding of particles deformed at their necks is then[33]

$$\dot{\varepsilon} = -\frac{\gamma_{sv}(1-\rho)}{r_p}\frac{D_l\Omega}{kTL^2} \tag{7}$$

The average distance between the dislocations in conventional size particles is much smaller than the particle size. Nevertheless, this distance becomes comparable to the nanoparticle size. Hence, in nanoparticle compacts, L may be replaced by the average nanoparticle radius.

Equations (6) and (7) are valid only when the pore surface is plastically deformed. The effective applied pressure (assuming hydrostatic pressing conditions within the die) needed for this deformation is then given by[35]

$$p_{limit} = \frac{2\sigma_{YP}}{3}\ln\left(\frac{1}{1-\rho}\right) \tag{8}$$

where σ_{YP} is the material yield point.

However, the contribution of the effective applied pressure on densification by rearrangement and plastic deformation should be added to equations (6) and (7).

MgO and NiO are very soft oxides; their single crystals are plastically deformable at room temperature. Therefore, these oxides can be used to demonstrate the densification behaviour of the plastic and soft nanoparticles that undergo yield during SPS. The SPS experiments showed that fully dense nanocrystalline NiO can be fabricated already at relatively low temperatures ($0{\cdot}48T_m$, where T_m is the melting temperature in K); sintering at 800°C and 100 MPa for 5 min resulted in 98% dense specimens.[36] The main densification and its maximum rate occurred during the heating and under the applied pressure (Fig. 3). This is in accordance with the theoretical expectations for densification of NiO by plastic deformation at relatively low temperatures. A simple calculation via equation (8) together with the yield stress data in Fig. 1 confirms that NiO can be densified to the density of over 98% at 800°C, with 100 MPa by plastic deformation (by dislocation glide). Full density was reached for an extended SPS duration of 20 min; the longer durations enabled additional diffusional processes (such as a dislocation climb or diffusional creep), which allowed complete densification of the compact.

However, when the effective applied pressure is below the yield stress, none or very limited plastic deformation is expected, which results in much lower densities. In this respect, SPS of NiO with the application of 25 MPa pressure at 550°C (below the yield stress of 37 MPa from room to 900°C[37]) resulted in 77·5% density, compared to 85·9% when 100 MPa pressure was applied.[31] Densification at pressures lower than needed for plastic deformation, appears to take place by particle sliding and rotation, without the contribution of plastic deformation. Although nanoparticle sliding and rotation increase the density by rearrangement/repacking, they eventually lead to sticking/bonding or even early neck formation; both effects can resist sliding and may result in lower final density.

Densification mechanism maps for 20 nm MgO nanoparticles showed that full densification by plastic deformation (assuming no coarsening and grain growth) can be obtained already under 100 MPa at 800°C ($0{\cdot}28T_m$) within 1 min.[38] Moreover, at a higher pressure of 200 MPa, a density of 96% can immediately be reached.[39] However, if grain growth is allowed during the first few minutes of densification, much larger durations are needed.

Higher temperatures usually result in higher densities due to the significant decrease in yield stress of the ceramic particles. Moreover, temperature increase leads to lower friction between the particles, which opposes sliding. However, the higher temperatures favour diffusional processes, and due to the exponential temperature dependence of the diffusion coefficients, this may result in grain growth and loss of the nanocrystalline character. Although an increase in the applied pressure is expected to enhance the densification, a high degree of plastic deformation may trigger recrystallisation at higher temperatures and loss of the nanocrystalline character. Consequently, the optimal pressure is needed to promote densification by neck flattening and at the same time prevent the significant strain hardening needed for recrystallisation.

In contrast to the extreme soft and hard ceramics, Y_2O_3 represents an intermediate behaviour between the

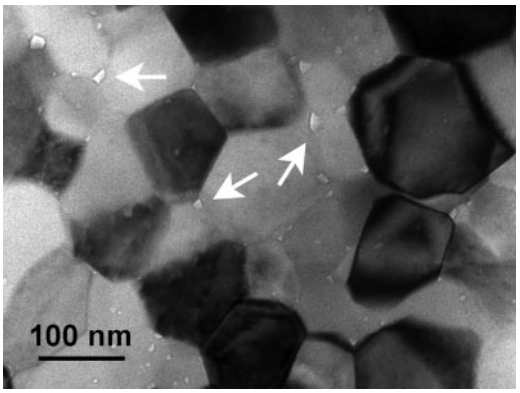

4 Image (TEM) of nanocrystalline Y_2O_3 sintered by SPS for 5 min at 1100°C and 100 MPa. Nanograins were dislocation free, but some LAGBs were present. Nanopores at grain corners were clearly visible (arrowed)

two cases. With a brittle to ductile transition at ~1000°C, it may serve as a hard or soft ceramic, depending on the temperature, pressure and average particle size. The SPS of nc-Y_2O_3 at 1100°C under 100 MPa for 20 min resulted in almost fully dense nanocrystalline specimens.[40] According to the recorded high densification rates, it was suggested that densification occurred mainly by grain sliding and rotation aided by surface diffusion. This was confirmed by TEM observations (Fig. 4), where the grain interior was dislocation free, but some LAGBs were found between the nanograins. The SPS of nc-Y_2O_3 at 100 MPa above 1400°C showed significant grain growth, where the large micrometre size grains were composed of subgrains with LAGBs; they resembled the annealed microstructure of the plastically deformed grains.[19,41] However, the nanocrystalline character could be preserved at the lower SPS temperatures as a result of the nanopore (arrowed in Fig. 4) drag on the GB mobility; this was confirmed by the theoretical calculations.[40]

Final stage sintering

At the final stage sintering, higher densities are achieved by the removal of inter- and intragranular porosities. The pores can shrink by the flux of vacancies from the pores (through the GBs or the lattice) to the compact surfaces. At this stage, densification occurs via diffusional processes, where GB diffusion has the largest effect, due to the large volume of GBs in nanocrystalline compacts. However, pore coarsening and grain growth during this sintering stage are very pronounced, through which the nanocrystalline character may be lost; full densification may be impeded as well. These processes are crucial particularly for nanocrystalline particles due to their high surface activities. The high heating rates used in SPS can limit grain growth and coarsening during heating, which significantly improves the ability to preserve the nanostructure.

Two apparent independent mechanisms are responsible for grain growth in nanocrystalline materials: grain coalescence by grain rotation and grain growth by GB migration; both mechanisms occur simultaneously and are enhanced under pressure, yet with different kinetics.[42]

Grain coalescence by grain rotation

Coalescence of nanograins may occur in the closed packed compact during the first and second stage sintering by particle sliding and rotation. The resultant nanograin clusters consist of LAGBs and hence are retained in a metastable state. Such nanograin clusters were observed in several SPS studies.[25,40] During the final stage sintering, grain coalescence occurs by diffusion accommodated nanograin rotation.[43] Neighbouring grains rotate by diffusional flow along the boundaries, while GB dislocations are absorbed at the GB mantel. The driving force is due to anisotropy in the surface energy, where high angle GBs are converted into LAGBs. The cluster growth rate by nanograin rotation, via GB diffusion, follows the R^{-4} dependence (where R is the grain radius).[43–45] Therefore, cluster growth by rotation is very fast for nanograins; but with increasing grain size, the growth rate drastically decays, so that it practically ceases for micrometre size grains. At SPS temperatures high enough for effective pipe diffusion, the LAGBs may be annealed out, resulting in the loss of the nanocrystalline character.

Grain growth

In pure systems, grain growth is controlled by the GB mobility and diffusion, perpendicular to the GB. The grain growth rate follows the R^{-1} dependence, which is much slower than the growth by nanograin coalescence. The growth rate decreases with the increase in grain size, albeit in a much moderate manner than that for the nanograin coalescence. Grain growth may be suppressed for the preservation of the nanostructure through structural features, such as nanopores or second phase particles; the pinning effect creates a drag on the moving GBs and limits their mobility. Nanopores were found to efficiently retard the grain growth in dense nanostructured ceramics subjected to SPS.[40,46,47]

Conclusion

It has been commonly observed that a significant portion of densification shrinkage takes place at the early and intermediate stages during SPS of ceramic nanoparticles. Unlike the densification occurring at the final stage of sintering, where slow interfacial diffusion of atoms always dominates, the densification achieved at these earlier stages is mainly reached by the rapid rearrangement and packing of nanoparticles, assisted by the applied mechanical pressure. This densification mechanism is essentially different from that dominating the same sintering periods during the conventional sintering, i.e. neck formation and neck growth. Depending on the elastic/plastic properties of nanoparticles, three categories of particle rearrangement and packing are demonstrated in rigid, deformable and semideformable nanoparticle systems. The temperature increase leads to a significant decrease in the yielding stress of the ceramic nanoparticles and in friction between the ceramic nanoparticles. Densification at pressures lower than needed for plastic deformation apparently takes place by particle sliding and rotation. Plastic deformation of ceramic nanoparticles contributes to the densification, when a pressure higher than the yielding stress of ceramic nanoparticles is applied.

References

1. H. Gleiter, J. Weissmuller, O. Wollersheim and R. Wurschum: 'Nanocrystalline materials: a way to solids with tunable electronic structures and properties?', *Acta Mater.*, 2001, **49**, (4), 737–745.
2. P. M. Derlet, R. Meyer, L. J. Lewis, U. Stuhr and H. Van Swygenhoven: 'Low-frequency vibrational properties of nanocrystalline materials', *Phys. Rev. Lett.*, 2001, **87**, (20), 205501.
3. R. Grossinger, R. Sato, D. Holzer and M. Dahlgren: 'Properties, benefits, and application of nanocrystalline structures in magnetic materials', *Adv. Eng. Mater.*, 2003, **5**, (5), 285–290.
4. M. A. Meyers, A. Mishra and D. J. Benson: 'Mechanical properties of nanocrystalline materials', *Prog. Mater. Sci.*, 2006, **51**, (4), 427–556.
5. L. Liu, Y. Li and F. H. Wang: 'Electrochemical corrosion behavior of nanocrystalline materials – a review', *J. Mater. Sci.*, 2010, **26**, (1), 1–14.
6. R. Orru, R. Licheri, A. M. Locci, A. Cincotti and G. Cao: 'Consolidation/synthesis of materials by electric current activated/assisted sintering', *Mater. Sci. Eng. R*, 2009, **R63**, (4–6), 127–287.
7. J. E. Garay: 'Current-activated, pressure-assisted densification of materials', *Ann. Rev. Mater. Res.*, 2010, **40**, 445–468.
8. Z. A. Munir, D. V. Quach and M. Ohyanagi: 'Electric current activation of sintering: a review of the pulsed electric current sintering process', *J. Am. Ceram. Soc.*, 2011, **94**, (1), 1–19.
9. R. Chaim, M. Levin, A. Shlayer and C. Estournés: 'Sintering and densification of nanocrystalline ceramic oxide powders: a review', *Adv. Appl. Ceram.*, 2008, **107**, (3), 159–169.
10. R. Chaim, Z. Shen and M. Nygren: 'Transparent nanocrystalline MgO by rapid and low-temperature spark plasma sintering', *J. Mater. Res.*, 2004, **19**, (9), 2527–2531.
11. P. Angerer, L. G. Yu, K. A. Khor and G. Krumpel: 'Spark-plasma-sintering (SPS) of nanostructured and submicron titanium oxide powders', *Mater. Sci. Eng. A*, 2004, **A381**, (1–2), 16–19.
12. Y. Zhou, K. Hirao, Y. Yamauchi and S. Kanzaki: 'Densification and grain growth in pulse electric current sintering of alumina', *J. Eur. Ceram. Soc.*, 2004, **24**, (12), 3465–3470.
13. R. Chaim: 'Densification mechanisms in spark plasma sintering of nanocrystalline ceramics', *Mater. Sci. Eng. A*, 2007, **A443**, (1–2), 25–32.
14. R. M. German: 'Particle packing characteristics', 121; 1989, Princeton, NJ, Metal Powder Industries Federation.
15. J. S. Reed: 'Principles of ceramics processing', 2nd edn, 427; 1995, New York, Wiley.
16. T. A. Ring: 'Fundamentals of ceramic powder processing and synthesis', 656; 1996, San Diego, Academic Press.
17. J. M. Valverde, M. A. S. Quintanilla and A. Castellanos: 'Jamming threshold of dry fine powders', *Phys. Rev. Lett.*, 2004, **92**, (25), 258303.
18. F. Q. Potiguar and H. A. Makse: 'Effective temperature and jamming transition in dense, gently sheared granular assemblies', *Eur. Phys. J. E*, 2006, **19E**, (2), 171–183.
19. R. Marder, R. Chaim, G. Chevallier and C. Estournés: 'Effect of 1 wt% LiF additive on the densification of nanocrystalline Y_2O_3 ceramics by spark plasma sintering', *J. Eur. Ceram. Soc.*, 2011, **31**, (6), 1057–1066.
20. L. T. Kuhn, R. M. McMeeking and F. F. Lang: 'A model for powder consolidation', *J. Am. Ceram. Soc.*, 1991, **74**, (3), 682–685.
21. K. Walton: 'The oblique compression of two elastic spheres', *J. Mech. Phys. Solids*, 1978, **26**, (3), 139–150.
22. S. Karato, Z. Wang and K. Fujino: 'High-temperature creep of yttrium–aluminum garnet single crystals', *J. Mater. Sci.*, 1994, **20**, (24), 6458–6462.
23. L. Mezeix and D. J. Green: 'Comparison of the mechanical properties of single crystal and polycrystalline yttrium aluminum garnet', *Int. J. Appl. Ceram. Technol.*, 2006, **3**, (2), 166–176.
24. R. Feldman, Y. Shimony, E. Lebiush and Y. Golan: 'Effect of hot acid etching on the mechanical strength of ground YAG laser element', *J. Phys. Chem. Solids*, 2008, **69**, (4), 839–846.
25. R. Chaim, R. Marder-Jaeckel and J. Z. Shen: 'Transparent YAG ceramics by surface softening of nanoparticles in spark plasma sintering', *Mater. Sci. Eng. A*, 2006, **A429**, (1–2), 74–78.
26. O. Tobi Even-Tzur and R. Chaim: 'Effect of green density and electric field direction on densification of YAG nano-powders by spark plasma sintering', *J. Mater. Sci.*, 2009, **44**, (8), 2063–2068.
27. N. Frage, S. Kalabukhov, N. Sverdlov, V. Ezersky and M. P. Dariel: 'Densification of transparent yttrium aluminum garnet (YAG) by SPS processing', *J. Eur. Ceram. Soc.*, 2010, **30**, (16), 3331–3337.
28. R. Chaim and Z. Shen: 'Grain size control by pressure application regime during spark plasma sintering of Nd-YAG nanopowders', *J. Mater. Sci.*, 2008, **43**, (14), 5023–5027.
29. V. M. Kenkre, M. R. Endicott, S. J. Glass and A. J. Hurd: 'A theoretical model for compaction of granular materials', *J. Am. Ceram. Soc.*, 1996, **79**, (12), 3045–3054.
30. Z. Shen, M. Johnsson, Z. Zhao and M. Nygren: 'Spark plasma sintering of alumina', *J. Am. Ceram. Soc.*, 2002, **85**, (8), 1921–1927.
31. R. Chaim, R. Reshef, G. Liu and Z. Shen: 'Low-temperature spark plasma sintering of NiO nanoparticles', *Mater. Sci. Eng. A*, 2011, **A528**, (6), 2936–2940.
32. J. X. Liu and D. P. DeLo: 'Particle rearrangement during powder compaction', *Metall. Mater. Trans. A*, 2001, **32A**, (12), 3117–3124.
33. W. Schatt and E. Friedrich: 'Self-activation of sintering processes in one-component systems', *Powder Metall. Int.*, 1981, **13**, (1), 15–20.
34. W. Schatt, Ju. I. Boiko, E. Friedrich and A. Scheibe: 'Shrinkage by particle sliding in sintering powder compacts', *Powder Metall. Int.*, 1984, **16**, (1), 9–11.
35. A. S. Helle, K. E. Easterling and M. F. Ashby: 'Hot-isostatic pressing diagrams: new developments', *Acta Metall.*, 1985, **33**, (12), 2163–2174.
36. R. Chaim and O. Reinharz Bar-Hama: 'Densification of nanocrystalline NiO ceramics by spark plasma sintering', *Mater. Sci. Eng. A*, 2010, **A527**, (3), 462–468.
37. A. Dominguez-Rodriguez, J. Casting and J. Philibert: 'Plastic deformation of pure and doped NiO single crystals', *Mater. Sci. Eng.*, 1977, **27**, (3), 217–223.
38. R. Chaim and M. Margulis: 'Densification maps for spark plasma sintering of nanocrystalline MgO ceramics', *Mater. Sci. Eng. A*, 2005, **A407**, (1–2), 180–187.
39. J. Reis and R. Chaim: 'Densification maps for spark plasma sintering of nanocrystalline MgO ceramics: particle coarsening and grain growth effects', *Mater. Sci. Eng. A*, 2008, **A491**, (1–2), 356–363.
40. R. Marder, R. Chaim and C. Estournés: 'Grain growth stagnation in fully dense nanocrystalline Y_2O_3 by spark plasma sintering', *Mater. Sci. Eng. A*, 2010, **A527**, (6), 1577–1585.
41. R. Chaim, A. Shelayer and C. Estournés: 'Densification of nanocrystalline Y_2O_3 ceramic powder by spark plasma sintering', *J. Eur. Ceram. Soc.*, 2009, **29**, (1), 91–98.
42. A. J. Haslam, D. Moldovan, V. Yamakov, D. Wolf, S. R. Phillpot and H. Gleiter: 'Stress-enhanced grain growth in a nanocrystalline material by molecular-dynamics simulation', *Acta Mater.*, 2003, **51**, (7), 2097–2112.
43. K. E. Harris, V. V. Singh and A. H. King: 'Grain rotation in thin films of gold', *Acta Mater.*, 1998, **46**, (8), 2623–2633.
44. D. Moldovan, D. Wolf and S. R. Phillpot: 'Theory of diffusion-accommodated grain rotation in columnar polycrystalline microstructures', *Acta Mater.*, 2001, **49**, (17), 3521–3532.
45. B.-N. Kim, K. Hiraga and K. Morita: 'Viscous grain-boundary sliding and grain rotation accommodated by grain-boundary diffusion', *Acta Mater.*, 2005, **53**, (6), 1791–1798.
46. B.-N. Kim, K. Hiraga, K. Morita, H. Yoshida, T. Miyazaki and Y. Kagawa: 'Viscous grain-boundary sliding with rotating particles or grains', *Acta Mater.*, 2009, **57**, (5), 1319–1326.
47. G. Bernard-Granger, C. Guizard and L. San-Miguel: 'Sintering behavior and optical properties of Y_2O_3', *J. Am. Ceram. Soc.*, 2007, **90**, (9), 2698–2702.